SEMARAK ILMU PUBLISHING

Journal of Advanced Research in Fluid Mechanics and Thermal Sciences

Journal homepage:
https://semarakilmu.com.my/journals/index.php/fluid_mechanics_thermal_sciences/index
ISSN: 2289-7879

A Stabilized Finite Element Formulation of Non-Newtonian Fluid Model of Blood Flow in A Bifurcated Channel with Overlapping Stenosis

Norliza Mohd Zain[1], Zuhaila Ismail[1,*], Peter Johnston[2]

[1] Department of Mathematical Sciences, Faculty of Science, Universiti Teknologi Malaysia (UTM), 81310 Johor Bahru, Johor, Malaysia
[2] Technology Building (N44), School of Environment and Science, Griffith University, Nathan, 4111 Queensland, Australia

ARTICLE INFO

Article history:
Received 19 May 2021
Received in revised form 1 September 2021
Accepted 9 September 2021
Available online 21 October 2021

Keywords:
Stabilized finite element; non-Newtonian; Galerkin least-squares; Overlapping stenosis; Bifurcated artery

ABSTRACT

A stabilized form of finite element formulation known as the Galerkin least-squares (GLS) method is implemented here for solving the two-dimensional incompressible non-Newtonian fluid model of blood flow in a diseased artery. The modelling for this type of flow is based on the conservation of mass and momentum equations, coupled with the generalised Newtonian liquid (GNL) constitutive equation characterized by the generalised power law (GPL) model. The flow of blood in this present study are assumed as steady, laminar and fully developed. The finite element algorithms considered herein are first solved for the Newtonian fluid in a straight artery with a bell shaped stenosis for validation purposes. As the efficiency and validity of the proposed algorithms are obtained through comparison with the findings from existing literature and COMSOL Multiphysics 5.2 software. Then, the algorithms are being implemented to the generalised power law fluid model of blood flow in a bifurcated artery with overlapping stenosis located at the parent's arterial lumen. The numerical results illustrate the arising of distinct sizes of vortex shedding downstream of the stenotic region for each generalised power law index.

1. Introduction

Finite element method (FEM) has been demonstrated as one of the most effective numerical methods for modelling the flow of blood which could be performed either in idealized or patient-specific models. This method also provides a faster rate of convergence for even large scale of transient simulations. Since that, Raptis *et al.,* [1] utilised the Galerkin weighted residual (GWR) method in generalised curvilinear coordinates to obtain the numerical solution for the non-linear system of governing equations which describes the blood flow in an aneurysmal geometry under the presence of a magnetic field.

However, as the classical Galerkin finite element formulation is employed to solve for a highly viscous incompressible fluid flow problem, the numerical instabilities like locking and spurious oscillations has emerged [2]. Due to the difficulties to impose the incompressibility constraint on the

* *Corresponding author.*
E-mail address: zuhaila@utm.my

https://doi.org/10.37934/arfmts.88.1.126139

flow field that may suffer from a spurious oscillation came from a standard Galerkin formulation, researchers then suggested a variety of stabilized FEM to solve these issues. In a stabilized finite element method, an additional term is added to the classical Galerkin formulation to enhance the accuracy of the Galerkin approach [3]. This added variational term is mesh-dependent, stable and consistent [3].

There are few stabilized finite element formulations to be implemented as alternatives to the basic Galerkin method in order to overcome the potential numerical instabilities. Among them are penalty FEM [4], Galerkin-least squares [5] and streamline upwind Petrov-Galerkin [3]. Heinrich *et al.,* [4] reviewed the penalty finite element method which is applied to Stokes and Navier-Stokes equations that can deal with incompressibility constraint and reducing number of the degrees of freedom by implicitly eliminating pressure as an unknown. Abdullah *et al.,* [6] with the helps of stabilization parameter which is added to the magnetic source term of the momentum equations are able to solve the numerical instability which arised in their solutions in a form of chaotic velocity vector. On the other hand, Skála *et al.,* [7], Machado *et al.,* [5] and Zinani *et al.,* [8], all employed Galerkin least-squares approach that was good deals with two major sources of problems in classical Galerkin formulation. The first one is the requirement to satisfy the inf-sup condition of Ladyzhenskaya-Babuska-Brezzi (LBB) condition to employ the combinations for the finite element interpolations for velocity and pressure fields [2,3]. Second is due to the inherent instability arising from the approximation of highly advective dominated flows by central difference schemes which may leads to spurious node-to-node oscillations [2,5,8].

Extensive studies previously and recently on different kind of models considered to represent the rheological behaviour of blood such as the generalised power law model [9-11], Carreau-Yasuda model [12], Casson model [13], power law model [14] as well as power law and Carreau models [15] to imitate the complex non-Newtonian characteristics of blood are presented. It is kind of impossible to capture a single constitutive relation that can predict all kinds of non-Newtonian behaviours of the fluid flowing in various situations, since the relation connecting the shear stress and the shear rate is non-linear [9,16]. For instance, the non-Newtonian behaviour of blood is more prominent at the region of low shear rates where the red blood cells are found clumped together into large particles (rouleaux) [17], causing the viscosity of blood to increase which usually forms in a region of smaller branches and capillaries [18]. The assumption as the non-Newtonian fluid exists also in the diseased conditions and in the pulsatile flow cases where the blood is dominated by cyclic low shear rates [17].

The most general model for non-Newtonian models was claimed by Ikbal *et al.,* [9] to be the generalised power law model due to its combination property of a Newtonian model at low shear rates, the power law model at high shear rates and the Casson model as a special case. Achaba *et al.,* [16] also approved the same fact as Ikbal *et al.,* [9] by considering a generalised power law model to constitute the non-Newtonian characteristics of blood since this model includes some classical models as a combination and generalization. It contains Newtonian behaviour at high shear rates and behaves as Casson and Carreau models as the special cases which are designed specifically to account for various haemodynamic factors which may affect the streaming blood [16]. For that reason, analysis by Achaba *et al.,* [16] concluded that generalised power law describes the blood viscosity at low shear rates better than the Cross and Newtonian models where the flow was found to be less distracted through the stenotic artery.

As far from the author's knowledge, there is no study from the previous literature on the GLS approximations of non-Newtonian cases solving for generalised power law model. Hence, different rheological model and arterial bifurcation are considered as the new contributions of this present study. The main focus of this current work is on the mathematical formulation that is involved in Galerkin least-squares method for solving the generalised Newtonian flow which is characterised as

a generalised power law model considering the shear-thickening as well as shear-thinning nature of blood. The streaming blood which is flowing through a bifurcated channel with overlapping stenosis is assumed to be steady, incompressible, laminar and fully developed. With the insight provided from previous GLS papers by Machado *et al.,* [5] and Zinani *et al.,* [8], we decided to implement this method to analyse the proposed problem considered herein considering that this method was well known with the benefits of overcoming the inherent instability arising from the approximation of highly advective dominated flows. In GLS, we also do not need to fulfil the compatibility combinations for velocity and pressure subspaces as stated in LBB condition. Therefore, the computational domain considered in this current work is discretized by using the continuous piecewise linear finite element spaces for all variables.

2. Governing Equations and Boundary Equations

We consider the steady-state, incompressible, fully developed, and laminar flow of blood which are constructed by incorporating the mass and momentum conservations as follow,

$$\begin{aligned} &\nabla \cdot \bar{\mathbf{u}} = 0 && \text{in } \bar{\Omega}, \\ &\rho \bar{\mathbf{u}} \cdot \nabla \bar{\mathbf{u}} - \nabla \cdot \bar{\tau} + \nabla \bar{p} = \rho \bar{\mathbf{f}} && \text{in } \bar{\Omega}, \end{aligned} \tag{1}$$

where $\bar{\mathbf{u}}$ is the velocity component, ρ is the density of blood, $\bar{\tau}$ is the stress tensor, $\bar{p}$ is the pressure or volumetric stress, $\bar{\mathbf{f}}$ is the dimensional body force vector and $\bar{\Omega}$ represent the domain. As mentioned before, in this study, we consider the generalised power law model which is a form of generalised Newtonian fluid which allow viscosity to vary with shear rate to represent the rheological behaviour of blood flow. According to Zinani *et al.,* [8] and Masud *et al.,* [18], by definition of the Generalised Newtonian Liquid (GNL) model, the stress tensor is the sum of volumetric stress and viscous stress components given as the constitutive equation that takes the form

$$\bar{\tau} = -\bar{p}\mathbf{I} + 2\eta(\dot{\gamma})\mathbf{D}, \tag{2}$$

where $\mathbf{I}$ is the unit tensor, $\eta(\dot{\gamma})$ is the viscosity function and $\mathbf{D}$ is the strain rate tensor which may be defined as

$$\mathbf{D} = \frac{1}{2}\left(\nabla \bar{\mathbf{u}} + \left(\nabla \bar{\mathbf{u}}\right)^{T}\right). \tag{3}$$

$\eta(\dot{\gamma})$ is dependent on the scalar $\dot{\gamma}$ that indicates the magnitude of the strain rate tensor given as

$$\dot{\gamma} = \sqrt{2D\left(\bar{\mathbf{u}}\right) : D\left(\bar{\mathbf{u}}\right)}. \tag{4}$$

GNL model allows the variation of viscosity with the shear rate. Thus, this model is useful in modelling the shearing flow and observing the effects of shear dominated flow under the natures of shear-thinning as well as shear-thickening [8]. The viscosity function, $\eta(\dot{\gamma})$ employed to Eq. (2) to model the shear dominated flows according to the generalised power law model can be written as

$$\eta(\dot{\gamma}) = -m\left|(I_2)\right|^{(n-1)/2}, \tag{5}$$

where m is the fluid consistency parameter, I_2 is the second invariant of the strain rate tensor and n is the power law index. In the case where the viscosity function $\eta(\dot{\gamma})$ in Eq. (5) is represented by a constant value of μ, Eq. (2) then reduces become a Newtonian viscosity model. In this study, we consider three cases of fluid's viscosities. The first one is the shear-thinning fluid indicated by the viscosity which is decreasing with an increase in shear rate represents by $n<1$. Then, we also consider the Newtonian fluid where $n=1$. Lastly, if $n>1$, then we obtained the shear-thickening fluid where the viscosity is increasing with an increase in shear rate. For two dimensional flow, the explicit form of I_2 is given as

$$I_2 = 2\left(\frac{\partial \bar{u}}{\partial \bar{x}}\right)^2 + 2\left(\frac{\partial \bar{v}}{\partial \bar{y}}\right)^2 + \left(\frac{\partial \bar{u}}{\partial \bar{y}} + \frac{\partial \bar{v}}{\partial \bar{x}}\right)^2. \tag{6}$$

Hence, the complete system of governing equations for the generalised power law fluid, plus the boundary conditions of prescribed velocity and forces in a domain $\bar{\Omega} \subset \mathrm{R}^2$ are given by

$$\begin{aligned}
&\nabla \cdot \bar{\mathbf{u}} = 0 && \text{in } \bar{\Omega},\\
&\rho \bar{\mathbf{u}} \cdot \nabla \bar{\mathbf{u}} - \nabla \cdot \left(2\eta(\dot{\gamma})\mathbf{D}\right) + \nabla \bar{p} = \rho \bar{\mathbf{f}} && \text{in } \bar{\Omega},\\
&\bar{\mathbf{u}} = \bar{\mathbf{u}}_g && \text{on } \bar{\Gamma}_g,\\
&\left(-\bar{p}\mathbf{I} + 2\eta(\dot{\gamma})\mathbf{D}\right)\mathbf{n} = \mathbf{t}_h && \text{on } \bar{\Gamma}_h,
\end{aligned} \tag{7}$$

where $\bar{\Gamma}$ is the boundary of the domain $\bar{\Omega}$, while $\bar{\Gamma}_g$ and $\bar{\Gamma}_h$ denotes part of the boundary $\bar{\Gamma}$, where Dirichlet and Neumann conditions are respectively imposed. $\bar{\mathbf{u}}_g$ is the prescribed boundary velocities, $\mathbf{n}$ is the unit outward normal vector and $\mathbf{t}_h$ is vector of the prescribed boundary tractions. Pressure point constraint are also employed as $\bar{p}(\bar{x}, \bar{y}) = 0$ $\bar{x} = 0.06\text{m}$, $\bar{y} = 0.017349\text{m}$ and $\bar{x} = 0.056175\text{m}$, $\bar{y} = -0.0239595\text{m}$.

Before proceeding to finite element implementation towards the system of governing equations as stated in Eq. (7), the proposed model has to be simplified first to non-dimensionalise all the units involved to reduce the complexity of the numerical formulation. These following non-dimensional terms are introduced for parameter rescaling as follows

$$x = \frac{\bar{x}}{\bar{h}},\ y = \frac{\bar{y}}{\bar{h}},\ u = \frac{\bar{u}}{\bar{u}_r},\ v = \frac{\bar{v}}{\bar{u}_r},\ p = \frac{\bar{p}}{\rho \bar{u}_r^2}, \tag{8}$$

where, the characteristic length, $\bar{h}$ refer to the length of the inlet. While, the reference velocity, $\bar{u}_r$ represents the average mean inflow velocity. Thus, by the non-dimensionalisation procedure the non-dimensional parameter of Reynolds number is attained as

$$\mathrm{Re} = \frac{\rho \bar{h}^n}{m \bar{u}_r^{n-2}}. \tag{9}$$

By the substitution of all the non-dimensional parameters specified in Eq. (8), Eq. (7) is transformed to its non-dimensional form given as

$$\begin{aligned}
&\nabla \cdot \mathbf{u} = 0 && \text{in } \Omega, \\
&\mathbf{u} \cdot \nabla \mathbf{u} - \frac{1}{\mathrm{Re}} \left|(I_2)\right|^{(n-1)/2} \nabla \cdot \mathbf{D} + \nabla p = \mathbf{f} && \text{in } \Omega, \\
&\mathbf{u} = \mathbf{u}_g && \text{on } \Gamma_g, \\
&(-p\mathbf{I} + \frac{1}{\mathrm{Re}} \left|(I_2)\right|^{(n-1)/2} \mathbf{D})\mathbf{n} = \mathbf{t}_h && \text{on } \Gamma_h.
\end{aligned} \tag{10}$$

The governing equations above are solved on two domains. The first one is a straight channel with bell shaped stenosis which was studied previously by Xenos *et al.,* [19] conducted as a test domain to verify the source code that is developed according to the GLS algorithms. For validation purposes of the first domain, the generalised power law index, n is taken as 1 to characterise the constant viscosity of μ for the Newtonian property of blood. As the efficiency and validity of the developed algorithms that is applied to the first domain has been achieved, then, we will implement the same algorithms to the second domain which is a bifurcated channel with constriction portrayed as an overlapping shaped. The domains involve in this particular study are shown in Figure 1 with the details on each domains can be clearly obtained from [20-22].

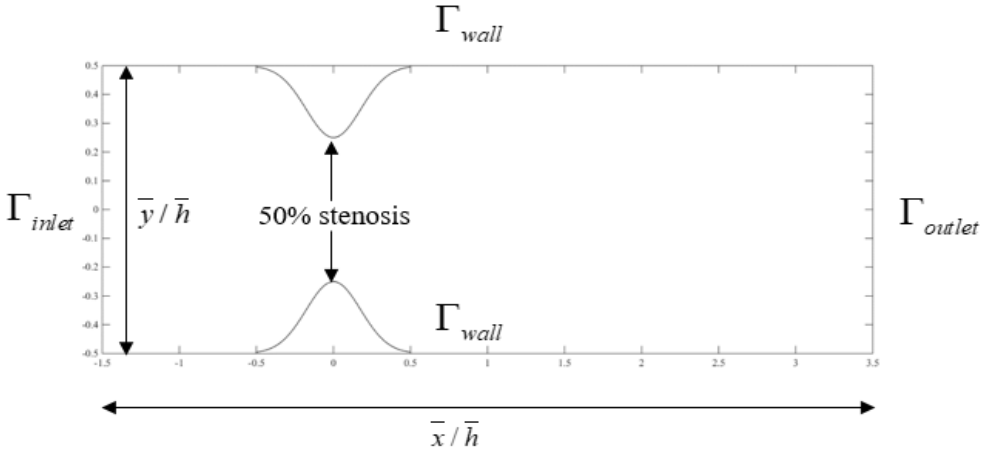

(a) Straight rectangular channel with bell shaped stenosis

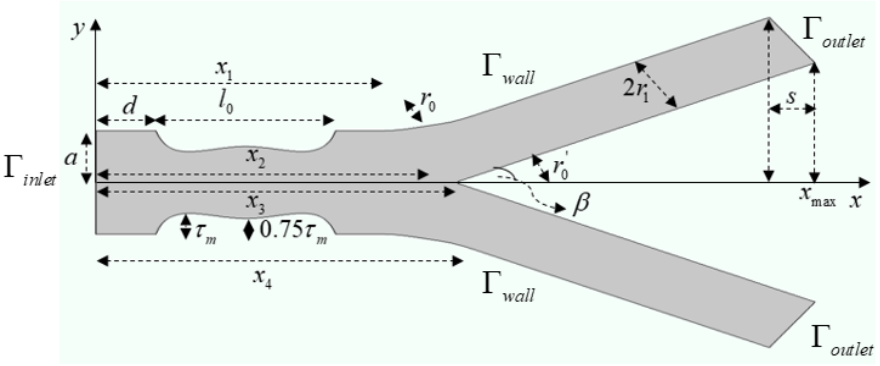

(b) Bifurcated channel with overlapping shaped stenosis

Fig. 1. Computational domains

The boundary conditions for the first domain can be obtained in details from previous literature by Xenos *et al.,* [19]. Meanwhile, the boundary conditions that are imposed to the second geometry are

$$
\begin{aligned}
&u = \frac{3}{2}\left(1 - \left(\frac{y}{1/2}\right)^{\frac{n+1}{n}}\right) \text{ and } v = 0, \text{ on } \Gamma_{inlet}, \\
&(-p\mathbf{I} + \tau)\mathbf{n} = 0, \qquad \text{on } \Gamma_{outlet}, \\
&u = 0 \text{ and } v = 0, \qquad \text{on } \Gamma_{wall}.
\end{aligned} \tag{11}
$$

The boundary condition specified in Eq. (11) is appropriate for generalised Newtonian fluid flow characterised by generalised power law model considering the shear-thinning, Newtonian and shear-thickening effects of blood.

3. Stabilized Finite Element Formulation

In this section, we present the stabilized finite element formulation of Galerkin least-squares method for the mathematical model presented in Eq. (10). Like in a common approach for the classical Galerkin finite element solution of a non-linear problem, in GLS the mesh-dependent term is added to the discretized boundary value problem to enhance the accuracy of the classical Galerkin approach [23]. Then, the Newton-Raphson method is applied to the non-linear algebraic system of equations to linearize the system. Meanwhile, the Gaussian quadrature technique is adopted to compute the numerical integrals presence in the systems.

3.1 Galerkin Least-Squares Formulation

To approximate the velocity and pressure components based on the usual fluid dynamics concept, the finite element subspaces for velocity and pressure fields over a finite element partition C_h of the problem domain Ω are defined as follow

$$
\begin{aligned}
&\mathbf{V}_h = \left\{\mathbf{N} \in \left[H_0^1(\Omega)\right]^2 \mid \mathbf{N}_{|\mathrm{K}} \in R_k(\Omega_K)^2,\ K \in C_h\right\}, \\
&\mathbf{V}_h^g = \left\{\mathbf{N} \in \left[H^1(\Omega)\right]^2 \mid \mathbf{N}_{|\mathrm{K}} \in R_k(\Omega_K)^2, \Omega_K \in C_h,\ \mathbf{N} = \mathbf{u}_g \text{ on } \Gamma_g\right\}, \\
&Q_h = \left\{p \in C^0(\Omega) \cap L_0^2(\Omega) \mid q_{|\mathrm{K}} \in R_l(\Omega_K)^2,\ \Omega_K \in C_h\right\}.
\end{aligned} \tag{12}
$$

The parameters R_k and R_l in Eq. (12) represent the polynomial spaces of degrees k and l, respectively defined over a finite element partition C_h of the problem domain Ω consisting of triangular element P_1 parametrized by a characteristic mesh size h_K. Based on the approximation functions define in Eq. (12), Galerkin least-squares formulation for boundary value problem introduced in Eq. (10) can be stated as to find $(\mathbf{u}_h, p_h)$ in the same vector space for all $(\mathbf{N}, q)$ which are also in the same vector space such that

$$
B(\mathbf{u}_h, p_h; \mathbf{N}, q) = F(\mathbf{N}, q),\ \forall (\mathbf{N}, q) \in (\mathbf{V}_h \times Q_h), \tag{13}
$$

where

$$B(\mathbf{u}_h, p_h; \mathbf{N}, q) = \int_\Omega \mathbf{u}\cdot\nabla\mathbf{u}\cdot\mathbf{N}d\Omega + \int_\Omega \frac{1}{\mathrm{Re}}\left|(I_2)\right|^{(n-1)/2}\mathbf{D}(\mathbf{u})\cdot\mathbf{D}(\mathbf{N})d\Omega - \int_\Omega p\nabla\cdot\mathbf{N}d\Omega$$
$$+\int_\Omega q\nabla\cdot\mathbf{u}d\Omega + \sum_{\Omega_{K\in C_h}}\int_{\Omega_K}\left[\begin{array}{c}\left(\mathbf{u}\cdot\nabla\mathbf{u}+\nabla p-\nabla\cdot\left(\frac{1}{\mathrm{Re}}\left|(I_2)\right|^{(n-1)/2}\mathbf{D}(\mathbf{u})\right)\right)\\ \cdot\left(\tau(\mathrm{Re}_K)\right)\left(\mathbf{u}\cdot\nabla\mathbf{N}+\nabla q-\nabla\cdot\left(\frac{1}{\mathrm{Re}}\left|(I_2)\right|^{(n-1)/2}\mathbf{D}(\mathbf{N})\right)\right)\end{array}\right]d\Omega_K, \tag{14}$$
$$F(\mathbf{N},q) = \int_\Omega \mathbf{f}\cdot\mathbf{N}d\Omega + \int_\Gamma \mathbf{t}_h\cdot\mathbf{N}d\Gamma$$
$$+\sum_{\Omega_{K\in C_h}}\int_{\Omega_K}\left[\mathbf{f}\cdot\left(\tau(\mathrm{Re}_K)\left(\mathbf{u}\nabla\cdot\mathbf{N}+\nabla q-\nabla\cdot\left(\frac{1}{\mathrm{Re}}\left|(I_2)\right|^{(n-1)/2}\mathbf{D}(\mathbf{N})\right)\right)\right)\right]d\Omega_K,$$

with the terms involved in Eq. (14) are counted elementwise with the positive parameter $\tau(\mathrm{Re}_K)$ behaves as a stabilization parameter throughout this study defined according to [5,8,24] as follow

$$\tau(\mathrm{Re}_K) = \frac{h_K}{2|\mathbf{u}|_2}\xi(\mathrm{Re}_K), \text{ where}$$
$$\mathrm{Re}_K = \frac{m_K\rho|\mathbf{u}|_2 h_K}{4\eta(\dot\gamma)},$$
$$|\mathbf{u}|_2 = \left(\sum_{i=1}^{2}|u_i|^2\right)^{1/2}, \tag{15}$$
$$\xi(\mathrm{Re}_K) = \begin{cases}\mathrm{Re}_K, 0\le\mathrm{Re}_K<1\\ 1, \mathrm{Re}_K\ge 1\end{cases},$$

$$\tau(\mathrm{Re}_K) = \frac{h_K}{2|\mathbf{u}|_2}\xi(\mathrm{Re}_K),$$
$$m_K = \min\{1/3, 2C_K\},\ h_K\|\Delta\mathbf{N}\|_{0,K}^2 \le C_K\|\nabla\mathbf{N}\|_0^2,\ \forall\mathbf{N}\in\mathbf{V}_h.$$

The terms h_K acts as the element size and $\eta(\dot\gamma)$ defined in Eq. (2), (7) and (15) represent the viscosity function for generalised power law model. The discretization of Eq. (13)-(15) are performed by substituting the trial functions $\mathbf{u}, p$ and $\mathbf{N}, q$ in terms of their finite element shape and weighting functions for linear triangular elements within an element $e_i, i = 1,2,3,\ldots,N_e$ that can be elucidated as

$$\mathbf{u} = \mathbf{u}^{e_i} = \mathbf{N}_j^{e_i}\mathbf{u}_j,$$
$$p = p^{e_i} = q_j^{e_i}p_j, \tag{16}$$

where $j = 1,2,3$ corresponding to three corner nodes per element e_i. By transforming Eq. (14) into its residual form, **R(U)** that can be written as

$$\mathbf{R}(\mathbf{U}) = \left[\mathbf{K}(\mathbf{U})\right]\mathbf{U} - \{\mathbf{F}\} = 0, \tag{17}$$

where $\mathbf{U}$ is vector for the degrees of freedom of $\mathbf{u}_h$ and p_h, $\mathbf{K}(\mathbf{U})$ stands for the stiffness matrices and $\{\mathbf{F}\}$ denotes the force vector. To deal with the non-linearity presented in Eq. (14), the Newton-Raphson method is implemented where the solutions are found converged at 10^{-4}. The convergence criteria τ of maximum residual, R_I norm is approximated as

$$\tau \leq \sqrt{\sum_{I=1}^{N} R_I^2}. \tag{18}$$

Hence, according to the Newton-Raphson method the solutions for the degrees of freedom are found as

$$\mathbf{U}^{b+1} = \mathbf{U}^b - \mathbf{J}^{-1}(\mathbf{U}^b)\mathbf{R}(\mathbf{U}^b), \tag{19}$$

where $\mathbf{J} = \partial\mathbf{R} / \partial\mathbf{U}$, that is also known as the Jacobian matrix and b is the iteration. Meanwhile, to approximate the integrals in Eq. (10), the Gaussian quadrature techniques are applied using six quadrature points throughout this study.

Based on the GLS formulations explained before, to sum up, these are the following algorithms that are applied in the developed source code by using the Matlab software

i. The domain geometry is constructed as in Figure 1. The finite element meshes are then generated from a "mesh2d" function developed by Darren Engwirda.
ii. The nodes and their edges are generated. The numbering for the variables defined at each node of the element are then employed for the global degree of freedoms $\{u, v, p\}$.
iii. The boundary conditions, convergence tolerance τ and all related parameters value are prescribed. The initial guess for $\{u, v, p\}$ is generated from the Stokes solution where n is made equal to 1.
iv. The element matrix is evaluated for each finite element where parameter n is set according to the rheological behaviour of fluid it supposedly present with the integrals computed using a Gaussian quadrature rule with the stabilization GLS terms calculated from Eq. (15).
v. The element matrices are then being assembled forming a global matrix and is solved subjected to the boundary conditions imposed as stated in Eq. (11).
vi. The residual $\mathbf{R(U)}$ in Eq. (17) is approximated.
vii. The convergence tolerance τ define in Eq. (18) is evaluated to check for the convergence of the solution. If this condition is fulfilled, then the iteration will stop and the solutions are obtained at the previous step.
viii. If the previous condition is not satisfied, then the Jacobian matrix $\mathbf{J}$ is evaluated.
ix. The solutions are corrected as $\mathbf{U}^{b+1} = \mathbf{U}^b \delta\mathbf{U}^b$ with $\delta\mathbf{U}$ appear to be $\delta\mathbf{U} = -\mathbf{J}^{-1}(\mathbf{U}^b)\mathbf{R}(\mathbf{U}^b)$.

As the solution of $\{u, v, p\}$ is acquired in the last iteration where the limit stated in step (vii) above has reached, then the iteration will stop.

4. Numerical Results and Discussions

An unstructured triangular mesh is used for all calculations in this study. For both geometries, continuous piecewise linear finite element basis functions are used for $\mathbf{u}$ and p. To verify that the source code developed is working properly according to the GLS algorithms, firstly, we need to

validate the source code that is developed using the Matlab software with the result that was obtained from the previous literature. After the verification has been achieved, then we will proceed the computation with the second domain of interest.

4.1 Straight Rectangular Channel With a Bell Shaped Stenosis - Test Domain

For the validation purpose, implementation into the Newtonian $(n=1)$ blood flow in a straight rectangular channel as studied by Xenos *et al.,* [19] is carried out in this study. From the mesh dependency test, we found that by using an unstructured triangular mesh of 21060 elements containing 10841 nodes, we are able to obtain a satisfactory solution and capable in capturing a good formation of vortex downstream of the stenotic region. The results are computed using $\mathrm{Re}=400, \rho=1050\mathrm{kgm}^{-3}$ and $\mu=0.0035\mathrm{kgm}^{-1}\mathrm{s}^{-1}$ which are found converged with $\tau=10^{-4}$.

The results for the maximum velocity and its location as well as the pressure drop at the centre of the stenosis are validated with the results obtained from Xenos *et al.,* [19] and Comsol multiphysics 5.2 software as tabulated in Table 1.

Table 1
Results for maximum u -velocity and its location and pressure drop

Results from	u -velocity and its location	∇p at $x=0$
Present study	1.5993 at (0.286,0)	0.7928
Xenos *et al.,* [19]	1.5360	0.8000
Comsol multiphysics 5.2	1.5789 at (0.2697,-0.0002)	-

Comparison of results that are made with the previous literature and COMSOL multiphysics software shows a small distinct of maximum u - velocity and its location. Meanwhile, the pressure drop evaluated from this current study shows an excellent agreement with the previous work. Overall, it can be concluded that the solutions are obtained in a satisfactory agreement between the previous work, COMSOL multiphysics, as well as the one computed from the source code, thus shows that the source code developed is working properly in a satisfactory manner.

4.2 Bifurcated Channel with an Overlapping Shaped Stenosis

The numerical simulation in this study is performed by considering the following parameters based on the data taken from [21] and [22]: $a=0.0075\mathrm{m}$, $l_0=0.015\mathrm{m}$, $d=0.005\mathrm{m}$, $x_{\max}=0.06\mathrm{m}$, $x_1=0.025\mathrm{m}$, $q=0.0002\mathrm{m}$, $\rho=1050\mathrm{kgm}^{-3}$, $\mu=0.0035\mathrm{kgm}^{-1}\mathrm{s}^{-1}$, $\beta=30^{\circ}$, $r_1=0.51a$, $h=2a$, and $\mathbf{f}=0$. Blood is assumed to behave as a generalised power law fluid model by considering the shear-thinning, Newtonian and shear-thickening natures of blood represented by generalised power law index of $n<1, n=1$ and $n>1$, respectively.

Mesh test was conducted onto the domain of interest with several number of meshes as illustrated in Figure 2 to verify that the results computed is independence of the number of mesh parameters. The results involving this type of computational domain are meshed using unstructured linear triangular elements by using the Reynolds number of $\mathrm{Re}=300$. The mesh dependency test perform here is carried out using the generalised power law index of $n=1$ which behaves as a Newtonian fluid.

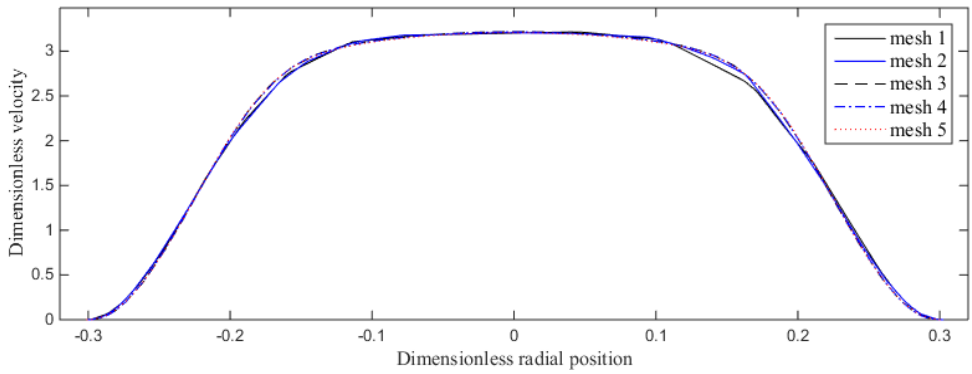

Fig. 2. The dimensionless axial velocity, u at the second throat of stenosis, $x=1$ for mesh 1 = 7787, mesh 2 = 10352, mesh 3 = 1 to , mesh 4= 17090 and mesh 5 = 28196

Based on the results plotted in Figure 2, the total number of elements between 11000-13000 are used to mesh the domain with the total number of 6000-8000 nodes that generated the degree of freedoms around 19000-23000, thus producing the global Jacobian and stiffness matrix of sizes 19000×19000 to 23000×23000. By the characteristics of mesh afore mentioned, Figure 3 illustrates the selected meshing used to mesh the stenosed bifurcated channel in this present study that is refined more at the stenotic region containing 12649 triangular elements.

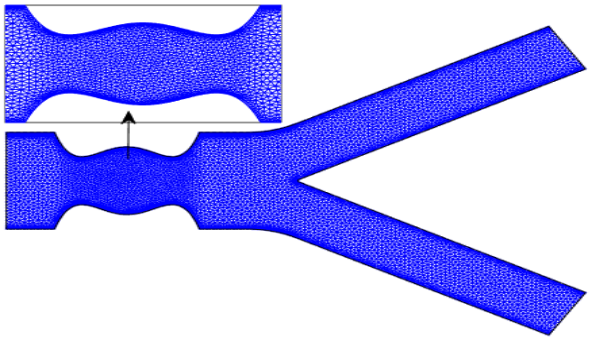

Fig. 3. The discretized bifurcated artery with refined mesh along the area of stenosis

Further, in Figure 4 and 5 the axial velocity profiles that are obtained at the second throat of an overlapping stenosis $(x=1)$ which is located at the mother artery and downstream of the stenotic region somewhere in the lower daughter branch $(x=3.0118)$ are respectively presented in these next figures. Based on Figure 4, the curves attaining a parabolic shape profiles with the velocity gradients that are gradually sloping as the generalised power law index, n is increased from 0.639 to 1.2. This might be due to the changes in apparent viscosity of fluids according to different generalised power law index, n that caused the shear-thinning fluid to flow faster and produce a largest flow reversal indicated by the negative valued velocities than its other counterparts.

Meanwhile, from Figure 5 it is also obviously seen from this current figure that the shear-thinning fluid forming the greatest flow reversal in comparison to Newtonian and shear thickening fluids. Apparently, the graphs for this three different fluids characterisation are skewed to the right because they are just passing through a region with a negative flow at the outer side of the arterial wall.

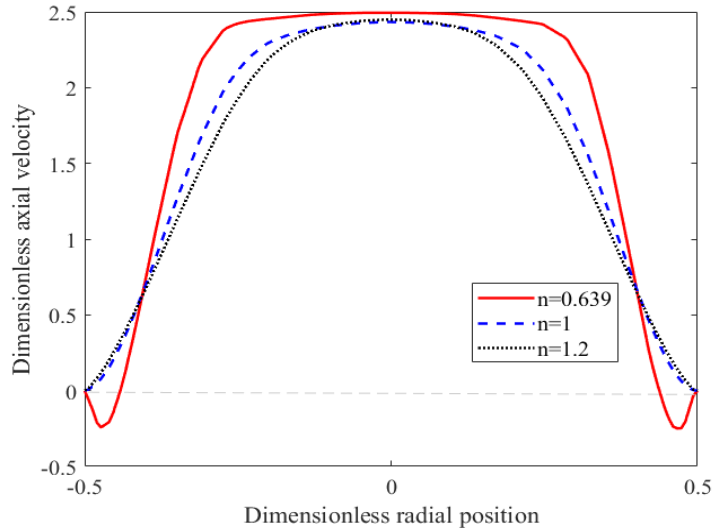

Fig. 4. Axial velocity profile at $x=1$ for different n

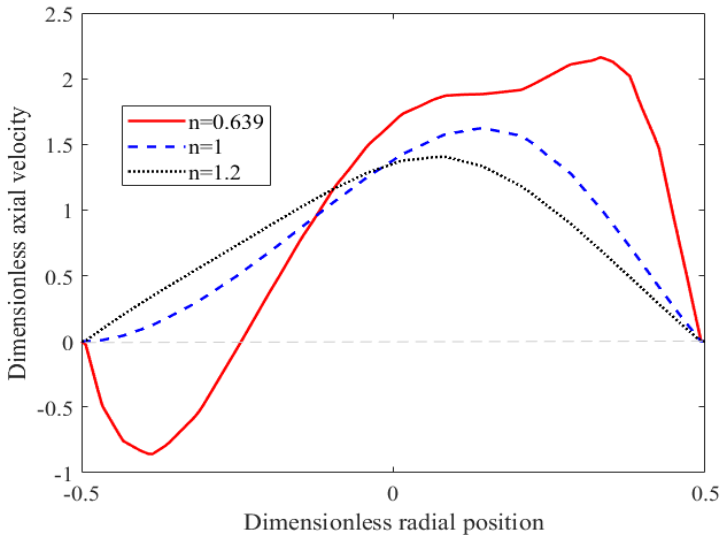

Fig. 5. Axial velocity profile at $x=3.0118$ for different n

The streamlines pattern for three different fluids characterisation are depicted as in Figure 6. It is discovered that the eddies formed by shear-thinning fluid downstream of an overlapping stenosis region near the upper and lower outer arterial wall are the largest. While for Newtonian case, the eddies formed is smaller than the one produced by shear-thinning fluid. Since shear-thickening fluid is the most viscous fluid over here, hence this fluid forms the smallest eddies in comparison with Newtonian and shear-thinning fluids. Among these three fluids, shear-thinning fluid moves faster and possesses a higher momentum. Thus, it is difficult for the same fluid layer to remain attached to suddenly changing geometry thus exhibits a more predominant vortex along the outer arterial wall.

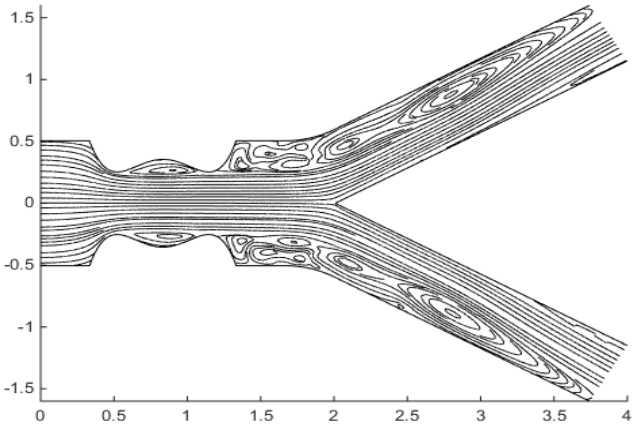

(a) $n = 0.639$

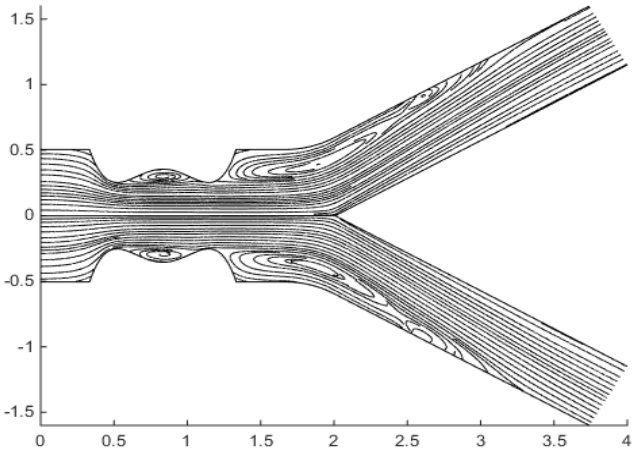

(b) $n = 1$

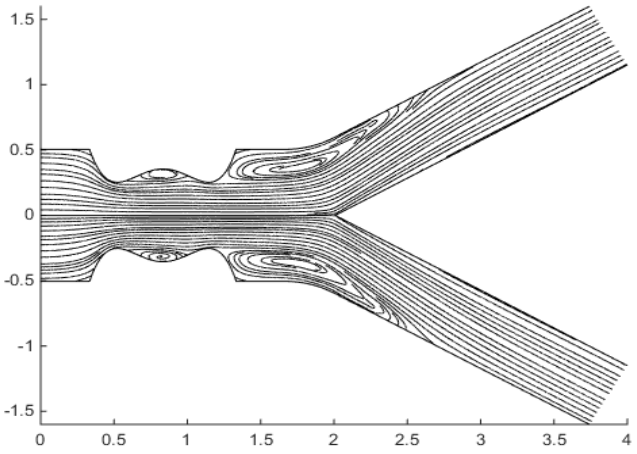

(c) $n = 1.2$

Fig. 6. Pattern of streamlines for different generalised power law index representing the fluids characterisation ($\mathrm{Re} = 300$ and $\tau_m = 0.4a$)

5. Summary and Conclusion

We have presented the stabilized finite element approach which is known as the Galerkin least-squares method to approximate the shear dominated flow characterised by the generalised power law index. As through the implementation of the classical Galerkin technique, we are failed to achieve the convergence of solution due to the arising of numerical instabilities as the flows are convection

dominated. Hence, in GLS, an additional stabilization parameter is added to the classical Galerkin formulation to enhance the accuracy of the computed solutions. By representing the generalised power law index, n according to various nature of blood which are $n=0.639$ for shear-thinning fluid, $n=1$ for Newtonian fluid and $n=1.2$ for shear-thickening fluid, the effects of different fluids characterisation that flowing through a bifurcated artery to the blood flow behaviours are examined in this papers. Comparisons that were made with reported findings in the literature and the one obtained from Comsol Multiphysics software show a satisfactory agreement between one another, thus convinced the applicability of the developed GLS algorithms in approximating the shear dominated flows in this study. Based on the numerical results obtained in the preceding section, it is obvious that the largest eddies are produced by the shear-thinning fluid $n=0.639$, followed by Newtonian fluid $n=1$, and the smallest eddies are created by the shear-thickening fluid $n=1.2$ corresponding to the changes in apparent viscosity as the generalised power law index is increasing.

Acknowledgements
The authors would like to acknowledge the Ministry of Higher Education and Research Management Centre, Universiti Teknologi Malaysia for the financial support and the authors are also grateful for the support and hospitality of the Sydney Mathematical Research Institute (SMRI) and Griffith university during preparing this work. This work was supported by the Ministry of Higher Education under Fundamental Research Grant Scheme FRGS/1/2019/STG06/UTM/02/21 and Research Management Centre, Universiti Teknologi Malaysia (UTM) under UTM Fundamental Research PY/2019/01623-Q.J130000.2554.21H48.

References

[1] Raptis, Anastasios, Michalis Xenos, Efstratios Tzirtzilakis, and Miltiadis Matsagkas. "Finite element analysis of magnetohydrodynamic effects on blood flow in an aneurysmal geometry." *Physics of Fluids* 26, no. 10 (2014): 101901. https://doi.org/10.1063/1.4895893

[2] Paramasivam, Vijayajothi, Nenad Filipovic, Kanesan Muthusamy, and Mohammed Rafiq Abdul Kadir. "Finite element computation for solving pulsatile blood flow: Relevance in assessing the flow dynamics in abdominal aortic aneurysms." *CFD Letters* 2, no. 4 (2010): 149-162.

[3] Rabby, Mir Golam, Rumia Sultana, Sumaia Parveen Shupti, and Md Mamun Molla. "Laminar blood flow through a model of arterial stenosis with oscillating wall." *International Journal of Fluid Mechanics Research* 41, no. 5 (2014). https://doi.org/10.1615/InterJFluidMechRes.v41.i5.30

[4] Heinrich, J. C., and Carlos A. Vionnet. "The penalty method for the Navier-Stokes equations." *Archives of Computational Methods in Engineering* 2, no. 2 (1995): 51-65. https://doi.org/10.1007/BF02904995

[5] Fernando Machado, Flávia Zinani, and Sérgio Frey. "Herschel-Bulkley Fluid Flows Through a Sudden Axisymmetric Expansion via Galerkin Least-Squares Methodology." 2007.

[6] Abdullah, Normazni, Zuhaila Ismail, Adrian Syah Halifi, Alia Rafiza Che Ayob, Erwan Hafizi Kasiman, and Norsarahaida Saidina Amin. "Numerical Computations of Biomagnetic Fluid Flow in a Lid Driven Cavity." *CFD Letters* 12, no. 4 (2021):43-53. https://doi.org/10.37934/cfdl.12.4.4353

[7] Skála, Jan, and Miroslav Bárta. "LSFEM implementation of MHD numerical solver." *Journal of Computational Physics* (2012). https://doi.org/10.4236/am.2012.331250

[8] Zinani, Flávia, and Sérgio Frey. "Galerkin least-squares solutions for purely viscous flows of shear-thinning fluids and regularized yield stress fluids." *Journal of the Brazilian Society of Mechanical Sciences and Engineering* 29 (2007): 432-443. https://doi.org/10.1590/S1678-58782007000400012

[9] Ikbal, Md A., S. Chakravarty, Kelvin KL Wong, Jagannath Mazumdar, and Prashanta K. Mandal. "Unsteady response of non-Newtonian blood flow through a stenosed artery in magnetic field." *Journal of computational and Applied Mathematics* 230, no. 1 (2009): 243-259. https://doi.org/10.1016/j.cam.2008.11.010

[10] Varshney, Gaurav, V. Katiyar, and Sushil Kumar. "Effect of magnetic field on the blood flow in artery having multiple stenosis: a numerical study." *International Journal of Engineering, Science and Technology* 2, no. 2 (2010): 967-982. https://doi.org/10.4314/ijest.v2i2.59142

[11] SHAIKH, AA, FH CHANDIO, and S. QURESHI. "Computation of Wall Shear Stresses Across Various Stenosis Length in Common Carotid Artery." *Sindh University Research Journal-SURJ (Science Series)* 47, no. 2 (2015): 367–370.

[12] Zaman, A., N. Ali, M. Sajid, and T. Hayat. "Effects of unsteadiness and non-Newtonian rheology on blood flow through a tapered time-variant stenotic artery." *AIP advances* 5, no. 3 (2015): 037129. https://doi.org/10.1063/1.4916043
[13] Lou, Zheng, and Wen-Jei Yang. "A computer simulation of the non-Newtonian blood flow at the aortic bifurcation." *Journal of biomechanics* 26, no. 1 (1993): 37-49. https://doi.org/10.1016/0021-9290(93)90611-H
[14] Stroud, J. S., S. A. Berger, and D. Saloner. "Numerical analysis of flow through a severely stenotic carotid artery bifurcation." *J. Biomech. Eng.* 124, no. 1 (2002): 9-20. https://doi.org/10.1115/1.1427042
[15] Alimohamadi, Haleh, Mohsen Imani, and Behjat Forouzandeh. "Computational analysis of transient non-Newtonian blood flow in magnetic targeting drug delivery in stenosed carotid bifurcation artery." *International Journal of Fluid Mechanics Research* 42, no. 2 (2015). https://doi.org/10.1615/InterJFluidMechRes.v42.i2.50
[16] Achaba, Louiza, Mohamed Mahfouda, and Salah Benhadida. "Numerical study of the non-Newtonian blood flow in a stenosed artery using two rheological models." *Thermal Science* 20, no. 2 (2016): 449-460. https://doi.org/10.2298/TSCI130227161A
[17] Papafaklis, Michail I., and Lampros K. Michalis. "Intravascular Imaging and Haemodynamics: The Role of Shear Stress in Atherosclerosis and In-Stent Restenosis." In *Intravascular Imaging: Current Applications and Research Developments*, pp. 326-348. IGI Global, 2012. https://doi.org/10.4018/978-1-61350-095-8.ch019
[18] Masud, Arif, and JaeHyuk Kwack. "A stabilized mixed finite element method for the incompressible shear-rate dependent non-Newtonian fluids: Variational Multiscale framework and consistent linearization." *Computer methods in applied mechanics and engineering* 200, no. 5-8 (2011): 577-596. https://doi.org/10.1016/j.cma.2010.08.012
[19] Xenos, M. A., and E. E. Tzirtzilakis. "MHD effects on blood flow in a stenosis." *Advances in Dynamical Systems and Applications* 8, no. 2 (2013): 427-437.
[20] Chakravarty, Santabrata, and Prashanta Kumar Mandal. "An analysis of pulsatile flow in a model aortic bifurcation." *International journal of engineering science* 35, no. 4 (1997): 409-422. https://doi.org/10.1016/S0020-7225(96)00081-X
[21] Chakravarty, S., and P. K. Mandal. "Mathematical modelling of blood flow through an overlapping arterial stenosis." *Mathematical and computer modelling* 19, no. 1 (1994): 59-70. https://doi.org/10.1016/0895-7177(94)90116-3
[22] Franca, Leopoldo P., Guillermo Hauke, and Arif Masud. "Revisiting stabilized finite element methods for the advective–diffusive equation." *Computer Methods in Applied Mechanics and Engineering* 195, no. 13-16 (2006): 1560-1572. https://doi.org/10.1016/j.cma.2005.05.028
[23] Jakub S´ıstek. "Stabilization of Finite Element Method for Solving Incompressible Viscous Flow." *Master's thesis Czech Technical University in Prague,* (2004).
[24] Franca, Leopoldo P., and Sérgio L. Frey. "Stabilized finite element methods: II. The incompressible Navier-Stokes equations." *Computer Methods in Applied Mechanics and Engineering* 99, no. 2-3 (1992): 209-233. https://doi.org/10.1016/0045-7825(92)90041-H